In-vitro biological evaluation of half sandwich platinum group metal complexes containing benzothiazole moiety

Lathewdeipor Shadap[a], Venkanna Banothu[b], Emma Pinder[c], Roger M. Phillips[c], Werner Kaminsky[d], Mohan Rao Kollipara[a*]

[a]Centre for Advanced Studies in Chemistry, North-Eastern Hill University, Shillong 793 022, India. E-mail: mohanrao59@gmail.com

[b]Centre for Biotechnology (CBT), Institute of Science & Technology (IST), Jawaharlal Nehru Technological University Hyderabad (JNTUH), Kukatpally-500 085, Hyderabad, Telangana State, India.

[c]Department of Pharmacy, School of Applied Sciences, University of Huddersfield, Queensgate, Huddersfield, HD1 3DH, UK

[d]Department of Chemistry, University of Washington, Seattle, WA 98195, USA

Graphical abstract

Reaction of halide bridged metal precursors of the platinum group with benzothiazole derivative ligands resulted in the formation of mononuclear N∩N cationic complexes. These complexes were characterized by various spectroscopic methods and screened for biological activity studies like antibacterial and cytotoxicity studies.

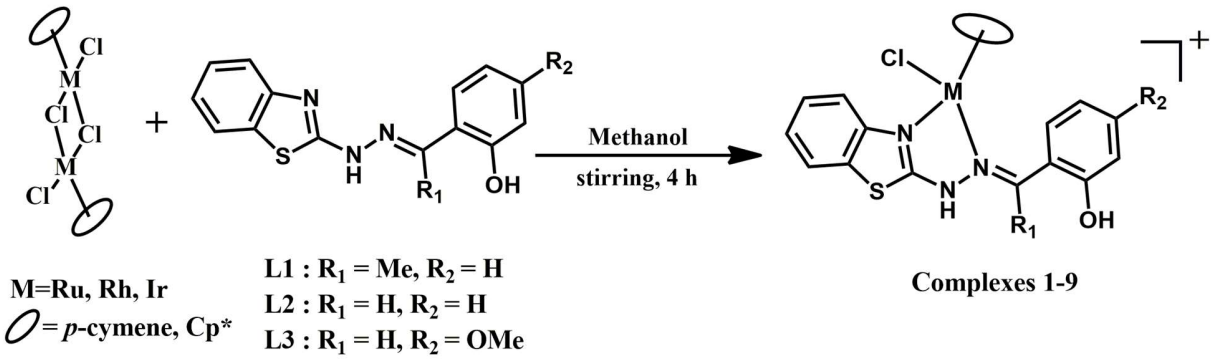

Abstract

Ligands containing benzothiazole moiety upon reaction with arene platinum group metal precursors in dry methanol yielded cationic complexes **1-9** having N∩N bonding mode. The general formulation of the complexes is presented as $[(arene)M(\kappa^2_{N\cap N}\text{-}L)Cl]^+$ where, L = **L1**, **L2** and **L3**, M = Ru, Rh and Ir, and arene = *p*-cymene and pentamethylcyclopentadiene (Cp*). All these complexes were characterized by various spectroscopic techniques and were found to be air-stable. The biological activity studies of these complexes and ligands such as antibacterial and cytotoxicity studies showed that complexes **5**, **6** and **9** have the highest antibacterial activity and ligand **L1** has the highest cytotoxicity activity.

Keywords: Ruthenium, rhodium, iridium, antibacterial, cytotoxicity.

1. Introduction

Schiff base metal complexes consisting of benzothiazole moiety still evoke an immense interest and possessed a variety of applications. Benzothiazole derivatives are a class of heterocyclic compounds with potent and momentous biological activities such as antitubercular, antibacterial, anti-inflammatory, anticonvulsant, antimalarial, anthelmintic, antileishmanial, antidiabetic, antidepressant and antitumor agents [1-8]. They also represent a wide range of coordinative properties due to the presence of additional donor sites; nitrogen, sulfur and oxygen atoms which serves as an important scaffold for the designing of new active compounds [9]. The incorporation of benzothiazole nucleus in metal complexes such as ruthenium, rhodium and iridium aimed at evaluating new products that possess interesting biological activities. 2-substituted benzothiazole derivatives as a core structure provides diversified therapeutically applications and the modification of the substituent at C-2 position of the benzothiazole ring results in varied bioactivity [10]. The biological and structural importance of the benzothiazole derivatives captured our interest to investigate their metal complexes.

The organometallic complexes of arene ruthenium, Cp*rhodium and Cp*iridium complexes [11, 12] are of great interest due to their potential anticancer activity [13-17] where some of the d^6-metal complexes have also been found to inhibit tumours by selective interactions with biomolecules. These complexes have also attracted much attention as antibacterial agents as well as anticancer agents [18, 19].

Colorectal cancer (CRC) has been reported to be the most common type of cancer worldwide. The development of new drugs is required to overcome drug resistance and DNA hypermethylation. So, in this study, two cancer cell lines HT-29 (colorectal carcinoma) and HCT-116 (colorectal carcinoma) have been taken and one non-cancer cell line ARPE-19 (human retinal epithelial cells) to evaluate the cytotoxicity of the compounds. Antibacterial activity study has been quite the common application of transition metal complexes, thereby in this study we are interested to learn about the potential activity of these complexes and ligands towards Gram-positive and Gram-negative bacterial strains.

Herein, we report the synthesis, characterization and biological activity studies such as antibacterial and cytotoxicity studies of arene metal complexes containing benzothiazole moiety. The ligands in this study have been prepared according to the reported procedure [19-21] and are presented in Chart 1.

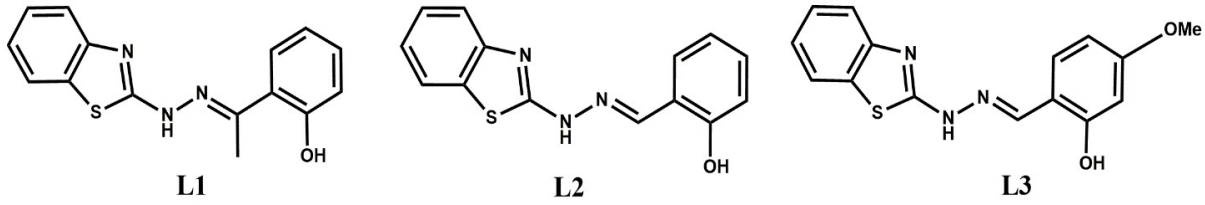

L1 **L2** **L3**

Chart 1: Ligands used in this study

2. Experimental

2.1. Materials and Methods

The reagents used in this study were of good commercial quality and used without further purification. α-phellandrene, pentamethylcyclopentadiene were purchased from Sigma Aldrich, 2-hydrazino benzothiazole, 2-hydroxy benzaldehyde, 2-hydroxy acetophenone and 2-hydroxy-4-methoxy benzaldehyde were purchased from Spectrochem, Alfa Aesar and S. D. fine Chem. Pvt. Ltd. The drying and distilling of the solvents were done in accordance with the standard procedures. Starting metal precursor $[(p\text{-cymene})Ru(\mu\text{-}Cl)Cl]_2$ was prepared according to the published procedures and $[Cp^*MCl_2]_2$ (M = Rh/Ir) were prepared using a synthesizer, Anton par mono-wave 50 [22].

The synthesized complexes were characterized by FT-IR, ^1H NMR, ^{13}C NMR, ESI-Mass, UV-Vis and single-crystal X- ray diffraction techniques. Infrared spectra (KBr pellets; 400-4000 cm^{-1}) of the synthesized compounds were recorded on a Perkin-Elmer 983 spectrophotometer, ^1H NMR and ^{13}C NMR spectra were recorded on a Bruker Advance II 400 MHz spectrometer using $CDCl_3$/DMSO-d_6 as the solvent and chemical shifts were referenced to TMS. Mass spectra were recorded with a Q-Tof APCI-MS instrument (model HAB 273) using acetonitrile as solvent. Absorption spectra were recorded on a Perkin-Elmer Lambda 25 UV-Vis spectrophotometer in the range of 200-600 nm in acetonitrile at room temperature.

2.2 Structure determination by X-ray Crystallography

To know about the bonding modes of the complexes, bond lengths and bond angles, suitable crystals were selected for crystallographic studies. The single crystal data for the complexes were collected using Oxford Diffraction Xcalibur Eos Gemini and Bruker AXS BV

Kappa CCD diffractometer with graphite monochromatic Mo-Kα radiation (λ = 0.71073 Å). The data collection was done using the CrysAlisPro CCD software. Crystal data was collected by standard ‘‘phi–omega scan’’ techniques and was scaled and reduced using CrysAlisPro RED software. The structure solution was carried out using SHELXT/SIR-92 and refined by a full-matrix least-squares method based on F^2 against all reflections using SHELXL-2014/7 and SHELXL-2016 [23]. The metal atoms were located from E-maps and all non-hydrogen atoms were refined anisotropically by full-matrix least-squares. Hydrogen atoms were placed in geometrically idealized positions and constrained to ride on their parent atoms with C-H distances in the range 0.95-1.00 Å. Isotropic thermal parameters U_{eq} were fixed such that they were 1.2 U_{eq} of their parent atom for CH's and 1.5 U_{eq} of their parent atom in case of methyl groups. The molecular structures were drawn using ORTEP-3 [24], packing pattern and interactions like π-π, H-bonding can be obtained using MERCURY [25]. Table **1** summarizes the crystallographic and structure refinement parameters for the represented complexes and selected bond lengths and bond angles are presented in Table **2**.

2.3 Antibacterial activity

All the Gram-positive and Gram-negative bacterial strains used in the present study were obtained from the Department of Microbiology, Osmania General Hospital, Hyderabad. All strains were tested for purity by standard microbiological methods. The bacterial stock cultures were maintained on Mueller-Hinton agar slants and stored at 4 ºC. An agar-well diffusion method [26] was employed for the evaluation of antibacterial activities of test compounds. DMSO was used as a negative control. The bacterial strains were reactivated from stock cultures by transferring into Mueller-Hinton broth and incubating at 37 ˚C for 18 hours. A final inoculum containing 10^6 colonies forming units (1 x 10^6 CFU/mL) was added aseptically to MHA medium and poured into sterile Petri dishes. Different test compounds at a concentration of 200 µg per well were added to wells (8 mm in diameter). Plates were incubated overnight at 37 ºC and the zone of inhibition was measured by considering the diameter around each well (mm). Experiments were performed in triplicates.

2.4 MIC and MIB

The minimum inhibitory concentration (MIC) and minimum bactericidal concentration (MBC) was determined by the micro-broth dilution method done in 96 well plates according to the standard protocol [27]. A two-fold serial dilution of the compounds, with appropriate antibiotic was prepared. Initially, 100 µL of MH broth was added to each well plate. Then 100 µL of compound or antibiotic was taken from the stock solution and dissolved in the first well plate. Serial dilution was done to obtain different concentrations. The stock concentrations of 2.0 mg/mL, 24 hour culture turbidity was adjusted to match 0.5 McFarland standards which correspond to 1×10^8 CFU/mL. The standardized suspension (100 µL) of bacteria was added to all the wells except the antibiotic control well and the 96 well plates were incubated at 37 °C for 24 hours. After 24 hours of incubation 40 µl of MTT (3-(4,5-dimethlthiazol-2-yl)-2,5-diphenyltrazolium bromide) reagent (0.1 mg/mL in 1x PBS) was added to all the wells. MIC was taken as the lowest concentration which did not show any growth which was visually noted from the blue color developed by MTT. Subcultures were made from clear wells and the lowest concentration that yielded no growth after subculturing was taken as the MBC.

2.5 Cell lines testing, culture condition and cytotoxicity studies

In this study, the response of HT29 and HCT116 p53 wild type ($p53^{+/+}$) cancer lines to the tested compounds using the MTT assay [28], was evaluated following a continuous 96-hours exposure. The activity of the compounds against cancer cells to non-cancer cells was studied by comparing against the retinal epithelium cell line ARPE-19. The cancer cells were kindly provided by Professor Bert Vogelsteins (John Hopkins University, Baltimore, MD) and ARPE-19 cells were originally purchased from ATCC. HT29 and HCT116 cells were routinely maintained as monolayer cultures in DMEM media supplemented with 10% fetal calf serum and L-glutamine (2 mM). ARPE-19 cells were routinely maintained as monolayer cultures in DMEM:F12 medium supplemented with 10% fetal calf serum, L-glutamine (2.5 mM) and sodium pyruvate (0.5 mM).

Using the MTT (3-(4,5-dimethylthiazol-2-yl)-2,5-diphenyltetrazolium bromide) cellular viability assay, the antiproliferative activity of the compounds was evaluated as described elsewhere [29]. Briefly, cells were seeded into 96 well plates at 2 x 10^3 cells per well and incubated for 24 hours at 37°C in an atmosphere of 5% CO_2 prior to drug exposure. Generally, a stock

solution of each compound was freshly prepared in DMSO at a concentration of 100 mM. The final DMSO concentration applied to cells was 0.1% (v/v), which is non-toxic to cells. The cells were exposed to a range of drug concentrations for 96 hours and cell survival was determined using the MTT assay. Following drug exposure, 20 µL of MTT (0.5 mg/mL) in phosphate-buffered saline was added to each well and it was further incubated at 37 °C for 4 hours in an atmosphere containing 5% CO_2. The solution was removed and formazan crystals were dissolved in 150 µM DMSO. The absorbance of the resulting solution was recorded at 550 nm using an ELISA spectrophotometer. The percentage of cell survival was calculated by dividing the true absorbance of treated cultures by the true absorbance for controls (exposed to 0.1% DMSO). Results are presented as the mean IC_{50} (µM) ± standard deviation for three independent experiments. The selectivity index (SI) was also calculated (defined as the IC_{50} for ARPE 19 cells divided by the IC_{50} for each cancer cell line) to compare the response of non-cancer cells to cancer cells. Values >1 indicate that compounds have selective activity against cancer compared to non-cancer cells *in-vitro*. Previously published data for cisplatin is also reported here to provide comparative results.

2.6 General procedure for the synthesis of metal complexes (1-9)

Metal precursors (0.1 mmol) on reaction with benzothiazole derivative ligands (**L1**, **L2** and **L3**) (0.2 mmol) and NH_4PF_6 (0.4 mmol) in dry methanol (10 mL), stirred at room temperature for 4 hours (Scheme 1). Upon completion of the reaction, the solution of the complexes were evaporated under reduced pressure and the residue was dissolved in dichloromethane (DCM), then filtered off the NH_4Cl formed through a bed of celite. The filtrates were reduced to about 2-3 mL and hexane was added to precipitate the desired complexes. While for the complex without NH_4PF_6 added, the solvent was fully evaporated and DCM was added to dissolve the residue and hexane was added to precipitate the desired complex. The complexes were washed with diethyl ether (twice) and air dried. Ruthenium complexes were yellowish-brown in color whereas rhodium and iridium complexes were orange-yellow colored complexes. All these complexes were found to be air-stable, non-hydroscopic and soluble in polar solvents like acetonitrile, chloroform, dichloromethane and insoluble in non- polar solvents like hexane, pet ether, *etc.*

2.6.1 [(p-cymene)Ru($\kappa^2_{N\cap N}$-L1)Cl]Cl (1)

Yield: (73%); dark yellow; FT-IR (KBr, cm^{-1}): 3450$\nu_{(N-H)}$, 1638$\nu_{(C=N)}$, 755$\nu_{(C-S)}$; ^{1}H NMR (400 MHz, $CDCl_3$ + DMSO-d_6, ppm) = 12.85 (s, 1H), 7.53 (d, 1H, *J* = 8 Hz), 7.45 (d, 1H, *J* = 8 Hz), 7.27-7.18 (m, 3H), 7.04 (t, 1H, *J* = 8 Hz), 6.95-6.88 (m, 2H), 5.71 (d, 2H, *J* = 8 Hz, $CH_{(p\text{-cym})}$), 5.67 (d, 2H, *J* = 8 Hz, $CH_{(p\text{-cym})}$), 3.04-2.94 (sept, 1H, $CH_{(p\text{-cym})}$), 2.55 (s, 3H), 2.24 (s, 3H, $CH_{(p\text{-cym})}$), 1.29 (d, 6H, *J* = 8 Hz, $CH_{(p\text{-cym})}$); ^{13}C NMR (100 MHz, $CDCl_3$ + DMSO-d_6, ppm) = 167.78, 164.19, 154.99, 147.51, 131.88, 131.59, 128.92, 127.68, 124.09, 122.69, 119.34, 117.68, 115.71, 30.67, 22.99, 22.56, 21.68, 18.94; MS-ESI (m/z): calculated: 519.09 $[M\text{-}PF_6\text{-}Cl]^+$, found: 518.27 $[M\text{-}PF_6\text{-}Cl\text{-}H]^+$; UV-Vis {$\lambda_{max}$ (nm), ε (10^{-4} M^{-1} cm^{-1})}: 211 (4.462), 350 (2.042).

*2.6.2 [Cp*Rh($\kappa^2_{N\cap N}$-L1)Cl]PF_6 (2)*

Yield: (78%); orange; FT-IR (KBr, cm^{-1}): 3444$\nu_{(N-H)}$, 1607$\nu_{(C=N)}$, 844$\nu_{(P-F)}$, 754$\nu_{(C-S)}$; ^{1}H NMR (400 MHz, $CDCl_3$, ppm) = 12.77 (s, 1H), 11.75 (s, 1H), 7.54 (d, 1H, *J* = 8 Hz), 7.48 (d, 1H, *J* = 8 Hz), 7.24 (t, 2H, *J* = 8 Hz), 7.18 (d, 1H, *J* = 8 Hz), 7.04 (t, 1H, *J* = 8 Hz), 6.93-6.87 (m, 2H), 2.54 (s, 3H), 1.71 (s, 15H, $CH_{(Cp^*)}$); ^{13}C NMR (100 MHz, $CDCl_3$ + DMSO-d_6, ppm) = 158.75, 158.33, 155.93, 144.21, 132.07, 131.64, 129.90, 129.25, 127.29, 126.40, 125.80, 123.93, 122.09, 121.20, 120.96, 118.69, 118.12, 116.56, 115.25, 111.91, 98.63, 95.93, 95.85, 22.92, 8.42; MS-ESI (m/z): calculated: 522.11 $[M\text{-}PF_6\text{-}Cl]^+$, found: 520.15 $[M\text{-}PF_6\text{-}Cl\text{-}2H]^+$; UV-Vis {$\lambda_{max}$ (nm), ε (10^{-4} M^{-1} cm^{-1})}: 221 (3.695), 352 (2.660).

*2.6.3 [Cp*Ir($\kappa^2_{N\cap N}$-L1)Cl]PF_6 (3)*

Yield: (72%); yellow; FT-IR (KBr, cm^{-1}): 3450$\nu_{(N-H)}$, 1605$\nu_{(C=N)}$, 845$\nu_{(P-F)}$, 756$\nu_{(C-S)}$; ^{1}H NMR (400 MHz, $CDCl_3$, ppm) = 12.79 (s, 1H), 7.52 (d, 1H, *J* = 8 Hz), 7.45 (d, 1H, *J* = 8 Hz), 7.32 (s, 1H), 7.24-7.23 (m, 2H), 7.06 (t, 1H, *J* = 8 Hz), 7.01 (d, 1H, *J* = 8 Hz), 6.95-6.88 (m, 1H), 2.53 (s, 3H), 1.75 (s, 15H, $CH_{(Cp^*)}$); ^{13}C NMR (100 MHz, $CDCl_3$, ppm) = 164.45, 155.49, 143.87, 132.89, 132.43, 130.02, 128.27, 127.09, 125.24, 125.11, 124.64, 122.84, 121.14, 119.90, 119.03, 117.73, 116.43, 88.83, 88.68, 86.92, 65.90, 23.61, 15.26, 8.91; MS-ESI (m/z): calculated: 612.17 $[M\text{-}PF_6\text{-}Cl]^+$, found: 610.22 $[M\text{-}PF_6\text{-}Cl\text{-}2H]^+$; UV-Vis {$\lambda_{max}$ (nm), ε (10^{-4} M^{-1} cm^{-1})}: 220 (3.199), 351 (2.465).

2.6.4 [(p-cymene)Ru($\kappa^2_{N\cap N}$-L2)Cl]PF_6 (4)

Yield: (80%); yellow; FT-IR (KBr, cm^{-1}): 3444$\nu_{(N-H)}$, 1632$\nu_{(C=N)}$, 847$\nu_{(P-F)}$, 758$\nu_{(C-S)}$; ^{1}H NMR (400 MHz, $CDCl_3$ + DMSO-d_6, ppm) = 10.73 (s, 1H), 8.39 (s, 1H), 7.58 (d, 1H, *J* = 8 Hz), 7.40 (d, 1H, *J* = 8 Hz), 7.29-7.24 (m, 3H), 7.07 (t, 1H, *J* = 8 Hz), 6.95-6.89 (m, 2H), 5.74 (d, 4H, *J* = 4 Hz, $CH_{(p\text{-cym})}$), 2.99-2.92 (sept, 1H, $CH_{(p\text{-cym})}$), 2.20 (s, 3H, $CH_{(p\text{-cym})}$), 1.27 (d, 6H, *J* = 8 Hz, $CH_{(p\text{-cym})}$); ^{13}C NMR (100 MHz, $CDCl_3$ + DMSO-d_6, ppm) = 161.91, 158.04, 157.14, 146.49, 133.13, 131.14, 128.49, 127.09, 123.76, 122.46, 120.20, 118.57, 117.29, 115.72, 83.97, 83.65, 30.28, 21.83, 21.36, 18.29; MS-ESI (m/z): calculated: 505.08 $[M\text{-}PF_6\text{-}Cl]^+$, found: 504.17 $[M\text{-}PF_6\text{-}Cl\text{-}H]^+$; UV-Vis {$\lambda_{max}$ (nm), ε (10^{-4} M^{-1} cm^{-1})}: 212 (3.816), 358 (1.444).

*2.6.5 [Cp*Rh($\kappa^2_{N\cap N}$-L2)Cl]PF_6 (5)*

Yield: (88%); orange; FT-IR (KBr, cm^{-1}): 3450$\nu_{(N-H)}$, 1628$\nu_{(C=N)}$, 844$\nu_{(P-F)}$, 756$\nu_{(C-S)}$; ^{1}H NMR (400 MHz, $CDCl_3$, ppm) = 10.85 (s, 1H), 8.38 (s, 1H), 7.55 (d, 1H, *J* = 4 Hz), 7.32 (d, 3H, *J* = 8 Hz), 7.14 (s, 1H), 7.03 (d, 2H, *J* = 8 Hz), 6.94 (t, 1H, *J* = 8 Hz), 1.71 (s, 15H, $CH_{(Cp^*)}$); ^{13}C NMR (100 MHz, $CDCl_3$ + DMSO-d_6, ppm) = 158.25, 155.23, 144.59, 134.27, 129.98, 129.14, 126.81, 123.85, 122.49, 119.38, 117.91, 117.57, 115.50, 98.89, 96.49, 96.41, 8.91; MS-ESI (m/z): calculated: 508.09 $[M\text{-}PF_6\text{-}Cl]^+$, found: 506.20 $[M\text{-}PF_6\text{-}Cl\text{-}2H]^+$; UV-Vis {$\lambda_{max}$ (nm), ε (10^{-4} M^{-1} cm^{-1})}: 221 (4.127), 353 (3.175).

*2.6.6 [Cp*Ir($\kappa^2_{N\cap N}$-L2)Cl]PF_6 (6)*

Yield: (79%); yellow; FT-IR (KBr, cm^{-1}): 3439$\nu_{(N-H)}$, 1629$\nu_{(C=N)}$, 845$\nu_{(P-F)}$, 757$\nu_{(C-S)}$; ^{1}H NMR (400 MHz, $CDCl_3$, ppm) = 10.88 (s, 1H), 8.37 (d, 1H, *J* = 12 Hz), 7.53 (d, 2H, *J* = 12 Hz), 7.31-7.28 (m, 3H), 7.11-7.07 (m, 1H), 6.99-6.90 (m, 2H), 1.74 (s, 15H, $CH_{(Cp^*)}$); MS-ESI (m/z): calculated: 598.15 $[M\text{-}PF_6\text{-}Cl]^+$, found: 596.13 $[M\text{-}PF_6\text{-}Cl\text{-}2H]^+$; UV-Vis {$\lambda_{max}$ (nm), ε (10^{-4} M^{-1} cm^{-1})}: 220 (3.880), 352 (3.152).

2.6.7 [(p-cymene)Ru($\kappa^2_{N\cap N}$-L3)Cl]PF_6 (7)

Yield: (81%); yellowish brown; FT-IR (KBr, cm^{-1}): 3450$\nu_{(N-H)}$, 1613$\nu_{(C=N)}$, 843$\nu_{(P-F)}$, 752$\nu_{(C-S)}$; ^{1}H NMR (400 MHz, $CDCl_3$, ppm) = 12.90 (s, 1H), 10.07 (s, 1H), 8.56 (d, 1H, *J* = 8 Hz), 8.15 (s, 1H), 7.61 (d, 1H, *J* = 8 Hz), 7.51-7.40 (m, 2H), 7.22 (t, 1H, *J* = 8 Hz), 7.16 (d, 2H, *J* = 8 Hz), 5.70 (s, 2H, $CH_{(p\text{-cym})}$), 5.40 (d, 2H, *J* = 4 Hz, $CH_{(p\text{-cym})}$), 3.84 (s, 3H), 3.09-3.03 (sept, 1H, $CH_{(p\text{-cym})}$), 2.00

(s, 3H, $CH_{(p\text{-cym})}$), 1.33 (d, 6H, J = 8 Hz, $CH_{(p\text{-cym})}$); ^{13}C NMR (100 MHz, $CDCl_3$ + DMSO-d_6, ppm) = 164.81, 161.07, 158.86, 150.21, 143.13, 130.74, 125.38, 124.82, 120.74, 120.64, 113.19, 111.14, 107.08, 105.55, 100.37, 99.55, 86.03, 84.90, 54.47, 29.55, 20.93, 17.47; UV-Vis {λ_{max} (nm), ε (10^{-4} M^{-1} cm^{-1})}: 201 (3.568), 291 (1.190), 372 (1.740).

*2.6.8 [Cp*Rh(κ²$_{N\cap N}$-L3)Cl]PF_6 (8)*

Yield: (85%); orange; FT-IR (KBr, cm^{-1}): 3440$\nu_{(N\text{-}H)}$, 1608$\nu_{(C=N)}$, 845$\nu_{(P\text{-}F)}$, 754$\nu_{(C\text{-}S)}$; ^1H NMR (400 MHz, $CDCl_3$, ppm) = 11.22 (s, 1H), 8.28 (s, 1H), 7.49 (d, 1H, J = 8 Hz), 7.41 (s, 1H), 7.24 (d, 1H, J = 8 Hz), 7.16 (d, 1H, J = 12 Hz), 7.06 (t, 1H, J = 8 Hz), 6.52-6.48 (m, 2H), 3.83 (s, 3H), 1.75 (s, 15H, $CH_{(Cp^*)}$); ^{13}C NMR (100 MHz, $CDCl_3$ + DMSO-d_6, ppm) = 163.74, 159.78, 156.72, 127.99, 124.28, 119.88, 119.43, 110.60, 104.51, 99.05, 96.82, 53.31, 6.66; MS-ESI (m/z): calculated: 538.10 $[M\text{-}PF_6\text{-}Cl]^+$, found: 536.06 $[M\text{-}PF_6\text{-}Cl\text{-}2H]^+$; UV-Vis {$\lambda_{max}$ (nm), ε (10^{-4} M^{-1} cm^{-1})}: 222 (3.885), 352 (3.378).

*2.6.9 [Cp*Ir(κ²$_{N\cap N}$-L3)Cl]PF_6 (9)*

Yield: (76%); light yellow; FT-IR (KBr, cm^{-1}): 3443$\nu_{(N\text{-}H)}$, 1627$\nu_{(C=N)}$, 845$\nu_{(P\text{-}F)}$, 753$\nu_{(C\text{-}S)}$; ^1H NMR (400 MHz, CDCl3, ppm) = 11.09 (s, 1H), 8.95 (s, 1H), 8.32 (s, 1H), 7.62 (s, 1H), 7.52-7.39 (m, 2H), 7.30-7.24 (m, 2H), 7.19 (broad singlet, 1H), 7.07 (t, 1H, J = 8 Hz), 3.83 (s, 3H), 1.74 (s, 15H, $CH_{(Cp^*)}$); MS-ESI (m/z): calculated: 628.16 $[M\text{-}PF_6\text{-}Cl]^+$, found: 627.15 $[M\text{-}PF_6\text{-}Cl\text{-}H]^+$; UV-Vis {$\lambda_{max}$ (nm), ε (10^{-4} M^{-1} cm^{-1})}: 223 (2.925), 351 (2.831).

3. Results and discussion

3.1 Synthesis of metal complexes

The metal complexes **1-9** in this study, were prepared according to Scheme 1. Ruthenium complexes were obtained as yellowish-brown colored compounds whereas rhodium and iridium complexes were obtained as orange to yellow colored compounds. Complexes were isolated as cationic complexes with PF_6^- as the counter ion except for complex **1** bearing Cl^- as the counter ion. In all these complexes, coordination to the metal centre takes place through the imine nitrogen and the nitrogen of the benzothiazole ring in a bidentate N∩N chelating fashion. All of these

complexes isolated were pure, quantitative yield, non-hygroscopic and air-stable. These complexes are also soluble in all polar solvents and insoluble in non-polar solvents.

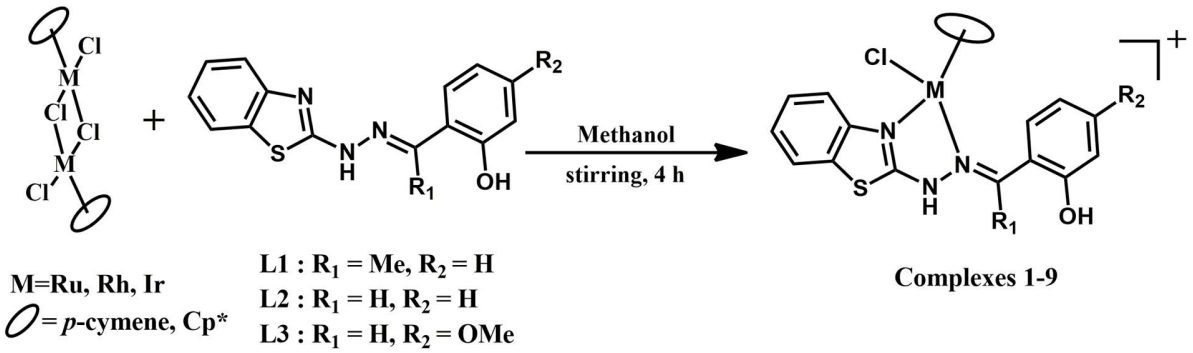

Scheme 1: Synthesis of metal complexes **1-9**

3.2 Spectral studies of complexes

3.2.1 Mass studies of the complexes

The mass analysis of the complexes was found to be in good correlation with the predicted formulation. The spectra of the representative complexes have been shown in the supplementary data (Figures S1-S8) and their values have been given in the experimental section. We observed that in addition to the molecular ion peaks, all the complexes except complexes **8** and **9** consist of isotopic mass peaks by the loss/gain of protons. Ruthenium complexes displayed their molecular ion peaks as $[M\text{-}2Cl\text{-}H]^+$ for complex **1** and $[M\text{-}PF_6\text{-}Cl\text{-}H]^+$ for complexes **4** and **7**. Rhodium and iridium complexes displayed their molecular ion peaks as $[M\text{-}PF_6\text{-}Cl\text{-}2H]^+$ except for complex **9** which corresponded to $[M\text{-}PF_6\text{-}Cl\text{-}H]^+$. This shows the formation of the complexes and that there is a strong bonding of the arene rings (arene = *p*-cymene, Cp*) to the metal atom.

3.2.2 FT-IR spectroscopy

In these synthesized metal complexes, the stretching frequencies of the N-H/O-H group were observed in the range 3439-3450 cm^{-1} comparable to that of the free ligands indicating that there is no bonding to the metal centre through (N-H) nitrogen or (O-H) oxygen atom. The stretching frequencies of C=N group in the case of free ligands were found to be in the range of

1604-1626 cm^{-1} while in the case of the complexes they were found to be in the range of 1607-1638 cm^{-1}. This small change in the stretching frequency of C=N of the complexes could be due to the delocalization of the electrons from the nitrogen donor atom upon coordination to the metal centres. In the case of the ligands, the C-S stretching frequencies were observed in the range 657-697 cm^{-1} while in the complexes the C-S stretching frequencies have increased and were observed in the range 752-758 cm^{-1}. This increase in the stretching frequency of C-S can be attributed to the delocalization of the electrons from the sulfur atom of the benzothiazole ring when coordination takes place through the nitrogen of the benzothiazole ring towards the metal centres. The presence of the counter ion PF_6^- in the cationic complexes can be observed at the range 843-851 cm^{-1}. These IR data gave us a preview of the composition and coordination of metal complexes by observing the prominent functional groups.

3.2.3 ^1H NMR studies of the complexes

The ^1H NMR spectra of the synthesized complexes have been provided in the supplementary information (Figures S9-S17). The N-H signals observed in the representative complexes were found to be in the range of 8.95-11.75 ppm. The O-H peak in all the complexes could prominently be observed in the range 10.73-12.90 ppm. All the ligand protons appeared in the aromatic region 6.48-8.56 ppm. The methyl protons of the complexes **1-3** were observed in the range 2.53-2.55 ppm while the methoxy protons of complexes **7-9**, occured in the range 3.83-3.84 ppm. In the case of ruthenium complexes (**1**, **4** and **7**), we noticed an unusual splitting pattern of the signal for *p*-cymene moiety. In complexes **1** and **7**, the aromatic proton signals of *p*-cymene split into two doublets accounting for two protons each at 5.71 ppm and 5.67 ppm (for complex **1**) and 5.70 ppm and 5.40 ppm (for complex **7**), while in the case of complex **4**, we observed only one doublet at 5.74 ppm accounting for four protons. This unusual pattern is due to the metal being a stereogenic centre and therefore, the aromatic and methyl isopropyl protons of the *p*-cymene ligand are diastereotopic when coordinated to the ligands [30]. A septet signal for the isopropyl proton was observed for complexes **1**, **4** and **7** at 3.04-2.94 ppm, 2.99-2.92 ppm and 3.09-3.03 ppm respectively and for the two methyl groups of the isopropyl moiety, we observed a typical doublet accounting for six protons at 1.29 ppm, 1.27 ppm and 1.33 ppm respectively. A singlet was observed for the methyl group of the *p*-cymene ring at the para position and this peak occurred at 2.24 ppm, 2.20 ppm and 2.00 ppm for complexes **1**, **4** and **7** respectively. For the rhodium and

iridium complexes, in addition to the proton signals of the ligands observed in the aromatic region, a sharp singlet around 1.71-1.75 ppm corresponding to Cp* protons was displayed. On the basis of these NMR data, the complexes synthesized were of good resonance and correlated with the expected formulation of the complexes.

3.2.4 ^{13}C NMR studies of the complexes

The spectra of the representative complexes have been given in the supplementary data (Figures S18-S24). The ^{13}C NMR spectra showed the aromatic carbon signals for the ligands around 167.78-110.60 ppm. In the case of complexes **7-9**, we observed the methoxy carbon signal appeared around 53.31-54.47 ppm. The *p*-cymene ring carbons were observed around 119.34-83.65 ppm while that of the methyl, methine and isopropyl carbons of the *p*-cymene ring were observed around 30.28-17.47 ppm. The methyl carbons of the Cp* ring were observed around 8.91-6.66 ppm and the carbons of the Cp* ring were observed at 99.05-86.92 ppm. Overall, these results support the formation of the complexes.

3.2.5 UV- Visible description of metal complexes

The electronic transition spectra of the metal complexes (**1-9**) have been provided in the supplementary data (Figure S25). This study was recorded in acetonitrile at room temperature. Since these d^6 complexes containing metal centres with filled d-orbitals of proper geometry, the electrons can occupy the empty low-lying π* orbitals of the ligands which may result in metal-to-ligand charge transfer (MLCT) transitions. Other from MLCT we also have π-π*/n-π* transitions due to the ligand part of the complexes. Metal-to-ligand charge transfer (MLCT) dπ(M) to π*(L) transitions can be assigned to the low energy absorption band observed in the range 291-358 nm while the high energy absorption band observed in the range 201-224 nm may be attributed to ligand-centred π-π*/n-π* transitions [31].

3.2.6 Description of molecular structures of metal complexes

In this study, we were able to establish the crystal structures of the represented metal complexes. The ORTEP diagrams of the isolated crystal structures **1** and **6** with atom numbering are presented in Figure 1 and the relevant crystallographic parameters along with the details of bond lengths, bond angles are listed in Tables 1 and 2. This study confirms the formation of the

complexes as cationic complexes bearing the general formula [(arene)M($\kappa^2_{N\cap N}$-L)Cl]$^+$. The molecular structures of these complexes revealed the respective ligands bind to the metal in a bidentate fashion through the imine nitrogen and the nitrogen of the benzothiazole ring leading to the formation of a five-membered chelated ring.

Complexes **1** and **6** crystallized in monoclinic system with space group *P21/n* and orthorhombic with space group *Pbca* respectively. The distance between the metal centre M(1) to centroid (CNT) of the arene/Cp* ring, metal to imine nitrogen M(1)-N(1), metal to benzothiazole M(1)-N(3) and metal to chloride M(1)-Cl(1) as well as the respective bond angles have been given in Table 2. The metal to chloride M(1)-Cl(1) and metal to nitrogen M(1)-N(1)/N(3) bond lengths found in these complexes are comparable to the previously reported values [32].

Molecular interactions like hydrogen bonding and covalent interactions stabilized the metal complexes. From the isolated molecular structures of the metal complexes, we observed inter-hydrogen bonding for complex **1** and complex **6** (Figure 2). In complex **1**, the observed inter-hydrogen distance between O(1)----H(9B) was found to be 2.670 Å while in complex **6**, we observed two inter-hydrogen interactions *i.e.*, between H(1)----Cl(1) and O(1)----H(23) distanced at 2.268 Å and 2.633 Å respectively.

3.2.7 In-vitro antibacterial assay

The ligands as well as the complexes were evaluated for their *in-vitro* antibacterial activity against Gram-positive; *Staphylococcus aureus* and Gram-negative; *Escherichia coli* and *Klebsiella pneumoniae* strains. The zone of inhibition (mm) in comparison with ciprofloxacin (positive control) was given in Figure 3 and Table S1. All the compounds exhibited potent antibacterial activity against the tested organisms. *In-vitro* assay results revealed that complex **5** (20 ± 1.06 mm), complex **6** (20 ± 1.18 mm) and complex **9** (20 ± 1.12 mm) have potent activity against Gram-positive (*Staphylococcus aureus*). Complex **5** (20 ± 0.92 mm), complex **6** (20 ± 1.08 mm) and complex **9** (19 ± 0.97 mm) also showed highest activity against Gram-negative (*Escherichia coli)* and also complex **5** (19 ± 0.86 mm), complex **6** (20 ± 1.13 mm) and complex **9** (18 ± 0.86 mm) showed activity against Gram-negative (*Klebsiella pneumoniae*). These antibacterial results suggested the potency of complexes **5**, **6** and **9** as antibacterial agents. Structurally, their potency in antibacterial activity could not be clearly understood as this may be

366 contributed by various factors such as the properties of the metal centres, orientation, lability and
367 also the substituents at the ligand moiety as well as the various physical conditions.

368 However, in comparison to the previous reported study on antibacterial activity of similar
369 benzothiazole compounds [33], one of the reason that these complexes/ligands under study are
370 potent could be the presence of a phenolic (-OH) group which has been reported to play a vital
371 role in antibacterial activity and other biological studies [34].

372 *3.2.8 Minimum inhibition concentration (MIC) and Minimum bactericidal concentration (MBC)*

373 The MIC and MBC results were listed in Figure 4 and Table S2. The MIC and MBC values
374 of the ligands and complexes ranged from 0.007 to 1.0 mg/mL against all three organisms. The
375 MIC and MBC values of complexes **2** and **3** ranged from 0.007 to 0.015 mg/mL. MIC and MBC
376 values of complexes **5** and **6** ranged from 0.062 to 0.125 mg/mL for *Staphylococcus aureus* and
377 *Escherichia coli* respectively and from 0.031 to 0.062 mg/mL for *Klebsiella Pneumoniae.*
378 Complex **9** showed MIC and MBC values ranging from 0.015 to 0.031 mg/mL for *Escherichia*
379 *coli* and from 0.007 to 0.015 mg/mL for *Klebsiella Pneumoniae.* The MIC and MBC values of
380 ciprofloxacin ranging from 0.031 to 0.062 mg/mL and 0.062 to 0.0125 mg/mL against the tested
381 organisms were taken as standard. These results suggested the high potency and efficient activity
382 of these complexes wih respect to ciprofloxacin.

383 *3.2.9 Cytotoxicity studies*

384 The biological application of the synthesized compounds could be further explored by
385 studying their cytotoxicity activies as well as that of cisplatin using cancer cell lines to meet the
386 development of new anticancer drugs. The activity values of the tested compounds against human
387 colorectal cancer cell lines HT29 and HCT116 $^{+/+}$ are presented in Figure 5 and Table S3. For both
388 HT29 and HCT116 $^{+/+}$ cell lines, IC_{50} values for the tested compounds ranged from 1.87 ± 0.083
389 (complex **4**) to 18.251 ± 0.219 µM (complex **7**). The response of non-cancer ARPE-19 cells ranged
390 from 1.268 ± 0.482 (complex **6**) to 35.011 ± 12.888 µM (ligand **L1**). From the cytotoxic studies,
391 complex **4** displayed more activity response towards the cancer cells studied at 1.87 ± 0.083 µM
392 (HT29) and 1.937 ± 0.05 µM (HCT116 $^{+/+}$) while complex **7** showed the least activity at 15.105 ±

393 0.424 μM (HT29) and 18.251 ± 0.219 μM (HCT116). The response of these tested compounds
394 cannot be clearly understood only that they have anticancer potency.

395 Selectivity indices (SI) of the tested compounds are presented in Figure 6 and Table S4. SI
396 value observed for Complex **9**, was slightly below 1 whilst the SI values for ligand **L1**, complexes
397 **1** and **2** obtained were above 1 which signified that these compounds have selective activity
398 towards both the cancer cells as to normal cells while complex **8** displayed selectivity only towards
399 HCT116 +/+ and not towards HT29. From this study, amongst the tested compounds, ligand **L1**
400 showed the highest SI and have superior potency *in-vitro*.

401 **4. Conclusion**

402 In summary, we have synthesized complexes of ruthenium, rhodium and iridium
403 containing benzothiazole derivative ligands. These complexes were characterized by various
404 spectroscopic techniques and by XRD analysis. The molecular structure revealed the coordination
405 of the ligands to the metal centre takes place through the imine nitrogen and the benzothiazole
406 nitrogen and forming a five-membered chelating ring. The antibacterial activity study done for the
407 ligands and complexes, against Gram-positive (*Staphylococcus aureus*) and Gram-negative
408 (*Escherichia coli* and *Klebsiella pneumoniae*) bacterial strains revealed good activity response,
409 from all the tested compounds with complexes **5**, **6** and **9** showing the highest activity. The ligands,
410 as well as the complexes, were also evaluated for cytotoxicity studies where all the tested
411 compounds exhibited anticancer activity with ligand **L1** displaying a superior activity compared
412 to the other compounds under study. The synthesized complexes portrayed the vast applications
413 of the platinum group metal complexes in the field of medicines and pharmaceuticals that could
414 be further taken up and studied at the molecular level.
415

References

[1] (a) R.S. Reshma, V.U. Jeankumar, N. Kapoor, S. Saxena, K.A. Bobesh, A.R. Vachaspathy, P.E. Kolattukudy, D. Sriram. *Bioorg. Med. Chem.,* **25**, 2761 (2017). (b) M. Bhat, S.L. Belagali. *Res. Chem. Intermed.,* **42**, 6195 (2016).

[2] A. Ahmadi, M. Khalili, H. Zandieh, B. Nahri-Niknafs. *Pharm. Chem. J.,* **49**, 530 (2015).

[3] N. Siddiqui, M.S. Alam, M. Sahu, M.J. Naim, M.S. Yar, O. Alam. *Bioorg. Chem.,* **71**, 230 (2017).

[4] S.S. Thakkar, P. Thakor, A. Ray, H. Doshi, V.R. Thakkar. *Bioorg. Med. Chem.*, **25**, 5396 (2017).

[5] A.M.M.E. Omar, O.M. Aboulwafa, D.A.E. Issa, M.S.M. El-Shoukrofy, M.E. Amr, I.M. El-Ashmawy. *Med. Chem. Commun.,* **8**, 1440 (2017).

[6] A.A. Dar, M. Shadab, S. Khan, N. Ali, A.T. Khan. *J. Org. Chem.,* **81**, 3149 (2016).

[7] A. Ahmadi, M. Khalili, L. Sohrabi, N. Delzendeh, B. Nahri-Niknafs, F. Ansari. *Mini Rev. Med. Chem.,* **17 (8)**, 721 (2017).

[8] L.W. Mohamed, A.T. Taher, G.S. Rady, M.M. Ali, A.E. Mahmoud. *Chem. Biol. Drug Des.,* **89**, 566 (2017).

[9] R.S. Keri, M.R. Patil, S.A. Patil, S. Budagumpi. *Eur. J. Med. Chem.,* **89**, 207 (2015).

[10] G. Akhilesh, R. Swati. *Asian J. Research Chem.,* **3(4)**, 821 (2010).

[11] E. Hilllard, A. Vessieres, F. Le Bideau, D. Plazuk, D. Spera, M. Huche, G. Jaouen. *Chem. Med. Chem.,* **1**, 551 (2006).

[12] M. Auzias, B. Therrien, G. Süess-Fink, P.P. Šteˇpnicˇka, W.H. Ang, P.J. Dyson. *Inorg. Chem.,* **47**, 578 (2008).

[13] A.F.A. Peacock, A. Habtemariam, R. Fernandez, V. Walland, F.P.A. Fabbiani, S.Parsons, R.E. Aird, D.I. Jodrell, P.J. Sadler. *J. Am. Chem. Soc.,* **128**, 1739 (2006).

[14] A. Habtemariam, M. Melchart, R. Fernandez, S. Parsons, I.D.H. Oswald, A. Parkin, F.P.A. Fabbiani, J.E. Davidson, A. Dawson, R.E. Aird, D.I. Jodrell, P.J. Sadler. *J. Med. Chem.,* **49**, 6858 (2006).

[15] M. Melchart, A. Habtemariam, O. Novakova, S.A. Moggach, F.P.A. Fabbiani, S. Parsons, V. Brabec, P.J. Sadler. *Inorg. Chem.,* **46**, 8950 (2007).

[16] M.A. Scharwitz, I. Ott, Y. Geldmacher, R. Gust, W.S. Sheldrick. *J. Organomet. Chem.,* **693**, 2299 (2008).

[17] S.K. Singh, S. Joshi, A.R. Singh, J.K. Saxena, D.S. Pandey. *Inorg. Chem.,* **46**, 10869 (2007).

[18] A.B.P. Rao, M. Kalidasan, K. Gangele, D.K. Deb, S.L. Shepherd, R.M. Phillips, K.M. Poluri, M.R. Kollipara. *Chemistry Select,* **2,** 2065 (2017).

[19] (a) R.K. Mohapatra, A.K. Sarangi, M.Azam, M.M. El-ajaily, Md. Kudrat-E-Zahan, S.B. Patjoshi, D.C. Dash. *J. Mol. Struct.,* **1179**, 65 (2019). (b) V.F.S. Pape, S. Toth, A. Füredi, K. Szebenyi, A. Lovrics, P. Szabo, M. Wiese, G. Szakacs. *Eur. J. Med. Chem.,* **117**, 335 (2016).

[20] (a) A.C. Pinheiro, M.V.N. de Souza, M.C.S. Lourenço, C.F.da Costa, T.C. Baddeley, J.N. Low, S.M.S.V. Wardell, J.L. Wardell. *J. Mol. Struct.,* **1178**, 655 (2019). (b) A. Pinheiro, M.N. de Souza, M.S. Lourenço, C.F. da Costa, T.C. Baddeley, J.N. Low, S.S.V. Wardell, J.L. Wardell. *J. Mol. Struct.,* **1178**, 655 (2019).

[21] (a) K.A. Maher, S.R. Mohammed. *Int. J. Cur. Res. Rev.,* **7**, 6 (2015). (b) H.M. Hesham, D.S. Lasheen, A.M.A. Khaled. *Archives of Pharmaceutical Sciences Ain Shams University,* **2 (1)**, 1 (2018).

[22] L. Shadap, S. Diamai, V. Banothu, D.P.S. Negi, U. Adepally, W. Kaminsky, M.R. Kollipara. *J. Organomet. Chem.,* **884**, 44 (2019).

[23] (a) G.M. Sheldrick. *Acta Crystallogr. Sect. A.* **64**, 112 (2008). (b) G.M. Sheldrick. *Acta Crystallogr. Sect. C.* **71**, 3 (2015).

[24] L.J. Farrugia. *J. Appl. Crystallogr.,* **45**, 849 (2012).

[25] C.F. Macrae, I.J. Bruno, J.A. Chisholm, P.R. Edgington, P. McCabe, E. Pidcock, L. Rodriguez-Monge, R. Taylor, J. van de Streek, P.A. Wood. *J. Appl. Cryst.,* **41**, 466 (2008).

[26] B. Venkanna, A. Uma, C. Suvarnalaxmi, N. Chandrasekharnath, R.S. Prakasham, L. Jayalaxmi. *Curr. Trends. Biotechnol. pharm.,* **7 (3)**, 782 (2013).

[27] V. Banothu, C. Neelagiri, U. Adepally, J. Lingam, K. Bommareddy. *Pharm Biol.,* **55**, 1155 (2017).

[28] Z. Almodares, S.J. Lucas, B.D. Crossley, A.M. Basri, C.M. Pask, A.J. Hebden, R.M. Phillips, P.C. McGowan. *Inorg. Chem.,* **53**, 727 (2014).

[29] M. Ahmadi, Z. Ahmadihosseini, S.J. Allison, S. Begum, K. Rockley, M. Sadiq, S. Chintamaneni, R. Lokwani, N. Hughes, R.M. Phillips. *Br. J. Pharmacol.,* **171(1)**, 224 (2014).

[30] K.T. Prasad, B. Therrien, M.R. Kollipara. *J. Organomet. Chem.,* **693**, 3049 (2008).

[31] S. Adhikari, W. Kaminsky, M.R. Kollipara. *J. Organomet. Chem.,* **848**, 95 (2017).

[32] L. Shadap, J.L. Tyagi, K.M. Poluri, E. Pinder, R.M. Phillips, W. Kaminsky, M.R. Kollipara. *Polyhedron,* **176**, 114293 (2020).

[33] L. Dkhar, W. Kamnsky, K.M. Poluri, M.R. Kollipara. *J. Organomet. Chem.,* **891**, 54 (2019).

[34] (a) M.K. Kim, J.C. Park, Y. Chong. *Nat. Prod. Commun.,* **7(1)**, 57 (2012). (b) M. Al-Mamary, S.I. Abdelwahab, H.M. Ali, S. Ismail, M.A. Abdulla, P. Darvish. *Asian. J. Chem.,* 24 (10), 4335 (2012).

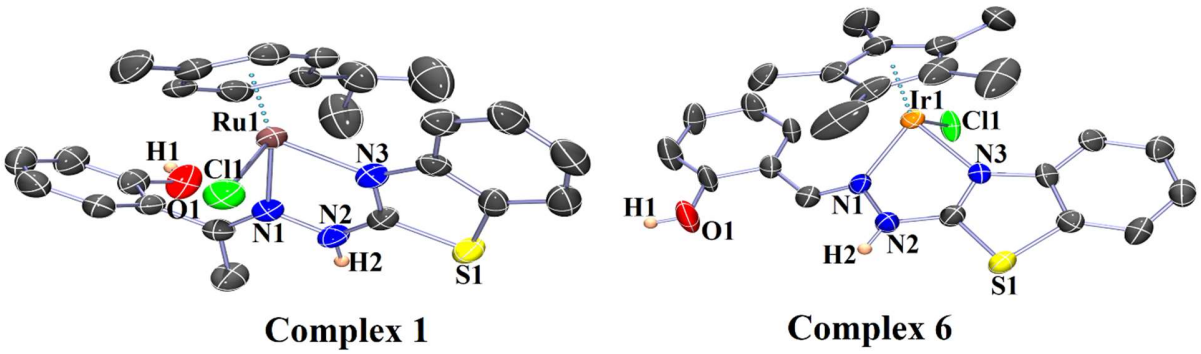

Complex 1 **Complex 6**

Figure 1: ORTEP diagrams of complexes **1** and **6** with 50% probability thermal ellipsoids. Hydrogen atoms (except NH and OH protons) and counter ions have been omitted for clarity.

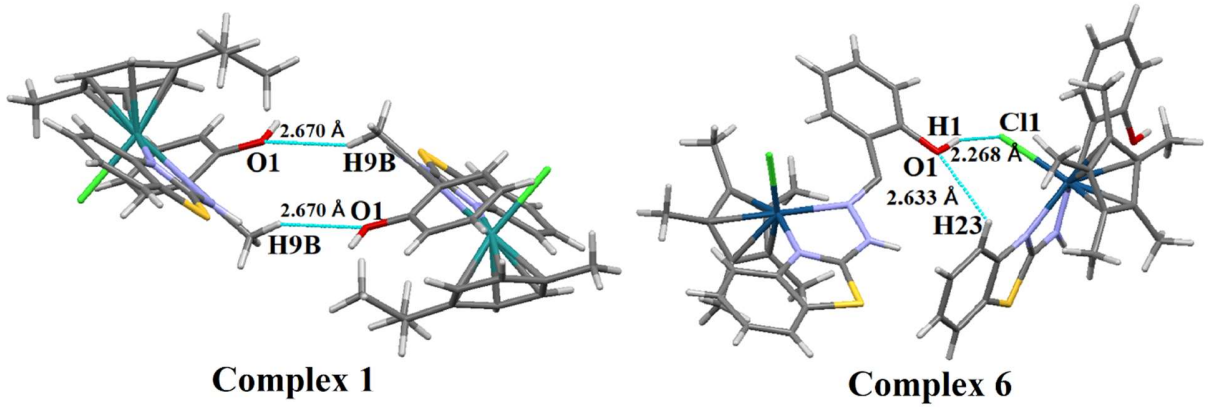

Complex 1 **Complex 6**

Figure 2: Inter H-bonding of complexes **1** and **6**. Complex **1** displayed interaction between O1----H9B (2.670 Å) and complex **6** between H1----Cl1 (2.268 Å) and O1----H23 (2.633 Å).

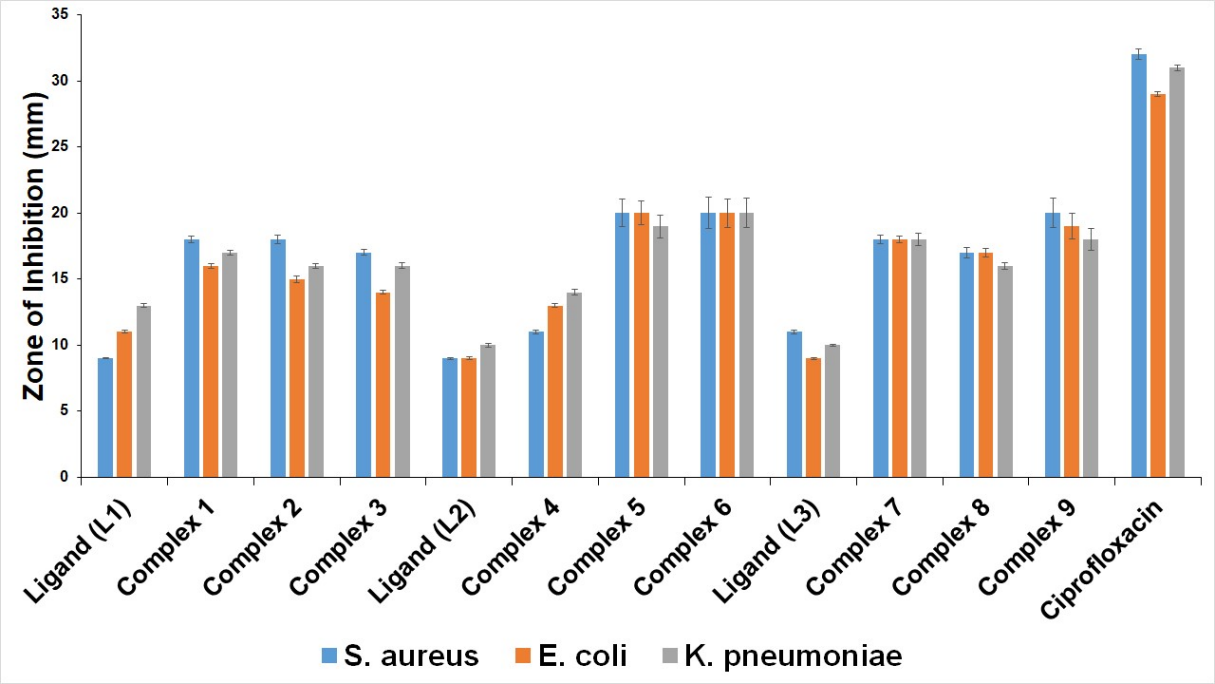

Figure 3: Antibacterial studies shown by ligands and complexes against Gram-positive and Gram-negative bacteria with ciprofloxacin as the reference.

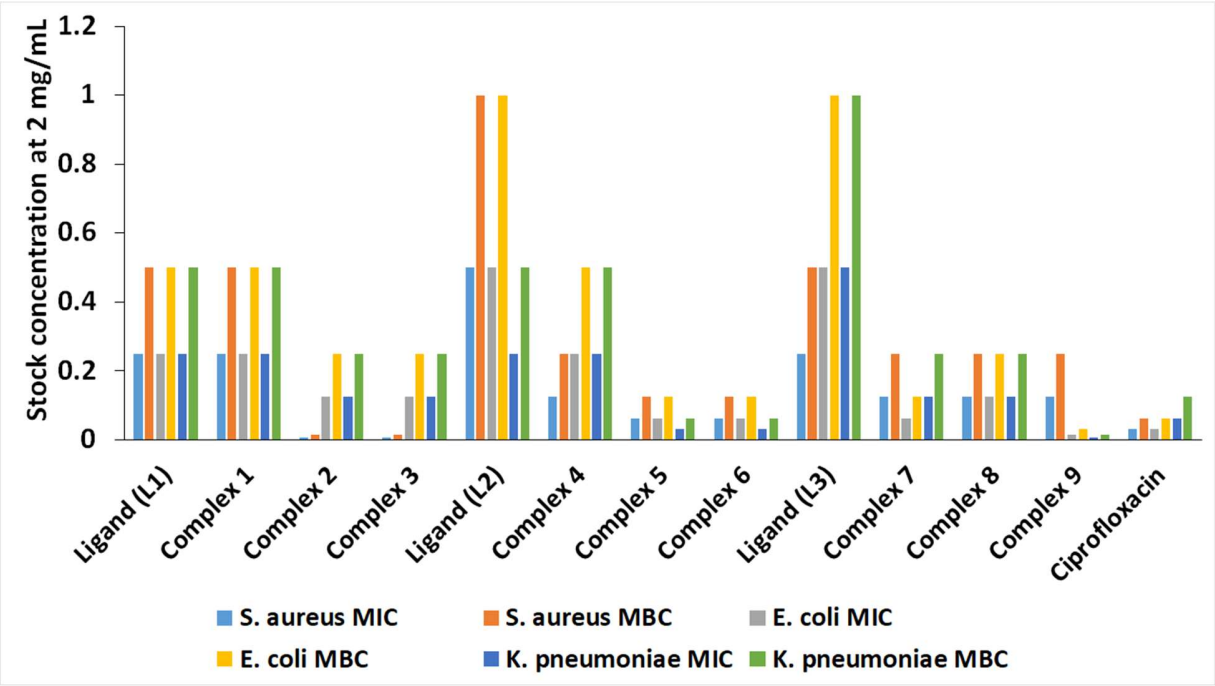

Figure 4: MIC and MBC of ligands and complexes.

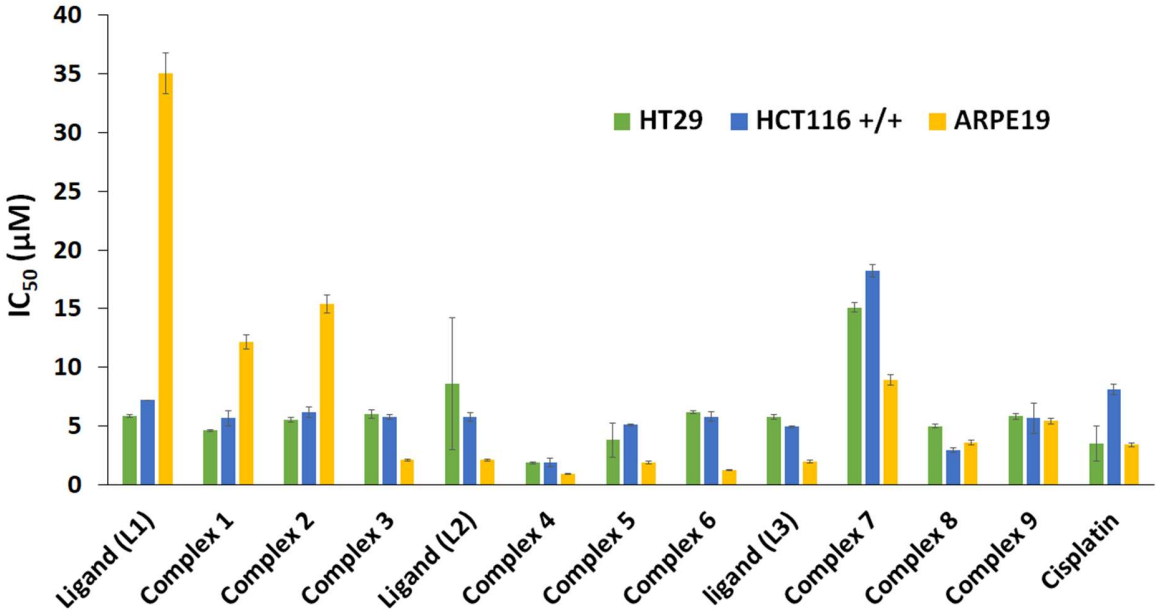

501

502 **Figure 5**: The response of cell lines following continuous 96-hour exposure. Each value represents
503 the mean IC_{50} value ± standard deviation for three independent experiments.

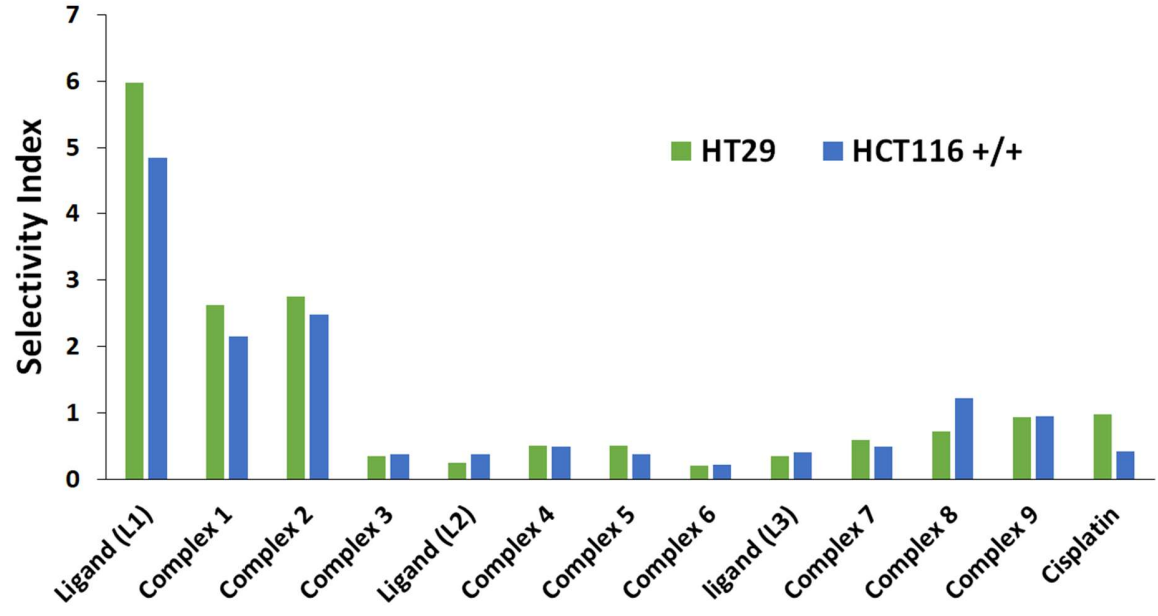

504

505 **Figure 6**: Selectivity indices for compounds and cisplatin. As these parameters were calculated
506 based upon the mean IC_{50} values, no error bars are presented here.

Table 1: Crystal structure data and refinement parameters of complexes **1** and **6**.

Complexes	[1] Cl	[6] PF_6
Empirical formula	$C_{27}H_{31}Cl_6N_3ORuS$	$C_{25}H_{27}Cl_3F_6IrN_3OPS$
Formula weight	759.38	861.07
Temperature (K)	292.6(3)	100(2)
Wavelength (Å)	0.71073	0.71073
Crystal system	monoclinic	orthorhombic
Space group	*P 21/n*	*P b c a*
a (Å)/α (°)	9.8542(8)/90	11.2100(2)/90
b (Å)/β (°)	27.989(2)/94.258(9)	18.5902(4)/90
c (Å)/γ (°)	11.8450(17)/90	29.4845(6)/90
Volume ($Å^3$)	3257.9(6)	6144.5(2)
Z	4	8
Density (calc.) (Mg/m^{-3})	1.548	1.862
Absorption coefficient	1.063	4.789
(μ) (mm^{-1})		
F(000)	1536	3352
Crystal size (mm^3)	0.26 x 0.21 x 0.09	0.30 x 0.24 x 0.21
Theta range for data collection (°)	4.0910 to 26.6170	2 to 20
Index ranges	-13<=h<=12, -37<=k<=19, -19<=l<=14	-14<=h<=14, -24<=k<=24, -39<=l<=39
Reflections collected	12803	13721
Independent reflections	7394 [R(int) = 0.0425]	7471 [R(int) = 0.0381]
Completeness to theta = 25.00°	99.60%	99.70%
Absorption correction	Semi-empirical from equivalents	Semi-empirical from equivalents
Refinement method	Full-matrix least-squares on F^2	Full-matrix least-squares on F^2
Data/restraints/parameters	7394/0/352	7471/5/398
Goodness-of-fit on F_2	1.136	1.152
Final R indices [I>2sigma(I)]	R1 = 0.0838, wR2 = 0.1740	R1 = 0.055, wR2 = 0.1166
R indices (all data)	R1 = 0.1181, wR2 = 0.1904	R1 = 0.0934, wR2 = 0.1311
Largest diff. peak and hole($e.Å^{-3}$)	0.883 and -1.104	1.992 and -1.692
CCDC.no	1985441	1985442

Structures were refined on F_0^2: $wR_2 = [\Sigma[w(F_0^2 - F_c^2)^2] / \Sigma w(F_0^2)^2]^{1/2}$, where $w^{-1} = [\Sigma(F_0^2)+(aP)^2+bP]$ and $P = [\max(F_0^2, 0)+2F_c^2]/3$

510 **Table 2**: Selected bond lengths (Å) and bond angles (°) of complexes **1** and **6**.

Complexes	1	6
M(1)-CNT	1.688	1.780
M(1)-N(1)	2.147(5)	2.130(7)
M(1)-N(3)	2.085(5)	2.090(7)
M(1)-Cl(1)	2.3944(18)	2.415(2)
N(1)-M(1)-Cl(1)	85.94(14)	90.3(2)
N(3)-M(1)-Cl(1)	83.87(15)	87.4(2)
N(1)-M(1)-N(3)	76.6(2)	76.1(3)

511 *CNT* represents the centroid of the arene/Cp* ring and (M = Ru, Rh and Ir).